Air-to-Fuel Ratio Control of Spark Ignition Engines Using Gaussian Network Sliding Control

Mooncheol Won, Seibum B. Choi, and J. K. Hedrick

***Abstract*—This paper treats air-to-fuel ratio control of a spark ignition engine. A direct adaptive control method using Gaussian neural networks is developed to compensate transient fueling dynamics and the measurement bias of mass air flow rate into the manifold. The transient fueling compensation method is coupled with a dynamic sliding mode control technique that governs fueling rate when the throttle change is not rapid. The proposed controller is simple enough for on-line computation and is successfully implemented on an automotive engine having a multiport fuel injection system.**

***Index Terms*— Air-to-fuel ratio control, Gaussian neural network, sliding mode control, spark ignition engine, transient fueling dynamics.**

I. Introduction

THE purpose of fuel injection control is to regulate the air-to-fuel (A/F) ratio at a desired ratio depending on the type of engine operations. These include warming up, constant high-speed operation, and the urban traffic mode which is characterized by frequent tip-in and tip-out movement of the throttle. Accurate regulation of desired A/F ratios will achieve the desired driveability, economic fuel consumption, and emission levels. The use of three-way catalytic converters are very common in most cars having spark ignition engines. The purpose of a catalytic converter is to oxidize excess levels of the tail pipe pollutants, such as CO, HC, and NO_X. Unfortunately, the efficiency of the catalytic converter is high enough only in a very narrow range around 14.64 (stoichiometry) of the A/F ratio as shown in Fig. 1. Therefore it is essential to maintain the A/F ratio close to the stoichiometry to reduce the pollutants. This paper will focus on regulation of the A/F ratio as close as possible around stoichiometry under the rapid changes of the throttle that characterize the urban traffic mode.

The A/F ratio regulation is a difficult control problem since the oxygen sensor at the exhaust gives almost binary information (leanness or richness of the A/F ratio as shown in Fig. 2), and has considerable sensing time delay [3]. There has been a great deal of research on transient air/fuel characteristics and its control [1], [2], [15], [15], [5], [17], and it is concluded that three characteristic delays are responsible for unwanted A/F ratio excursions during transient operations. These are the time-delay of the computer control system, a transport delay in the intake manifold, and a physical delay of the fuel flow which results from the finite rate of evaporation of the fuel film on the intake manifold and port walls.

Many of the current production fuel injection controllers utilize feedforward control based on a mass air flow sensor located upstream of the throttle plus a proportional integral (PI) type feedback control with look-up tables which require a laborious process of calibration and tuning to be built are difficult to apply since they need the output magnitude information which is not available in the A/F ratio control.

As a solution to this problem, Cho and Hedrick proposed a sliding mode fuel-injection control method [6], [7]. This analytic design method is in good agreement with the binary nature of the oxygen sensor signal. However, the method has the problem of large amplitude chattering which is due to the unavoidable oxygen sensor time-delay. The chattering problem limits the magnitude of the feedback gain; however, an appropriate amount of gain is required to guarantee the surface attraction condition under the existence of modeling errors. Choi and Hedrick suggested a dynamic sliding mode control method which combines the traditional "speed-density" and "mass-air-flow-meter" methods, and reduces the chattering considerably [8], [9]. Numerical simulation results show the effectiveness of the method under considerable sensor time delay. However the controller is effective only when the throttle change is not rapid, since the controller depends mainly on feedback sensor information. When the throttle angle changes abruptly, which means the air flow rate into the cylinder changes fast, the feedback sensor with time delay can not sense the abrupt change of the air flow rate. In this paper, a new transient fueling compensation technique is developed to regulate A/F ratio when the throttle changes fast [21]. The developed controller is a combination of feedforward and feedback control that utilizes a direct adaptive sliding control method with Gaussian neural networks [16].

The mass air flow rate into the manifold can be measured by hot wire or film sensors, and the sensor characteristics changes with temperature and aging. Therefore, the measurement is biased with temperature and aging. The bias in the measurement of the mass air flow rate into the manifold is also adapted on-line by the oxygen sensor and a Gaussian neural network. The advantage of this method is its robustness to engine aging and individual engine characteristics by using on-line adaptation.

This paper is organized as follows. In Section II, a fuel injection model for control is presented. In Section III, the structure of the fuel injection controller is presented. Section IV explains the dynamic sliding mode control. Section V introduces a direct adaptive control method utilizing Gaussian functions. Section VI deals the compensation of the measurement bias of

Manuscript received October 23, 1996. Recommended by Associate Editor, J. Winkelman.

M. Won is with the Department of Mechatronics Engineering, Chungnam National University, Taejon, Korea 305-764.

J. K. Hedrick is with the Department of Mechanical Engineering, University of California at Berkeley, Berkeley, CA 94720 USA.

S. B. Choi is with Light Vehicle Braking Systems, Livonia, MI 48150–2172 USA.

Publisher Item Identifier S 1063-6536(98)06250-2.

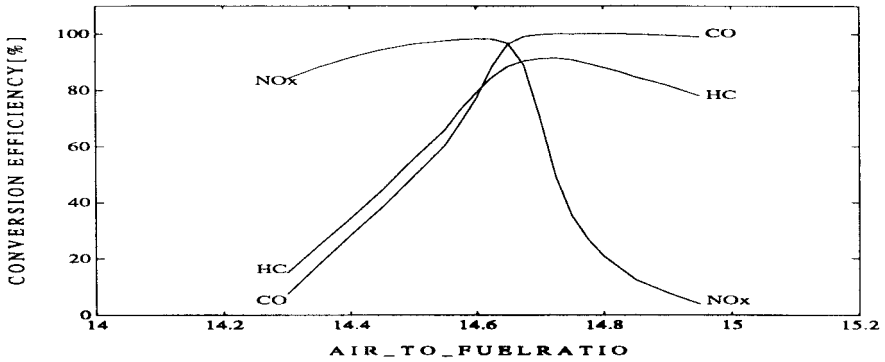

Fig. 1. A typical catalytic converter efficiency.

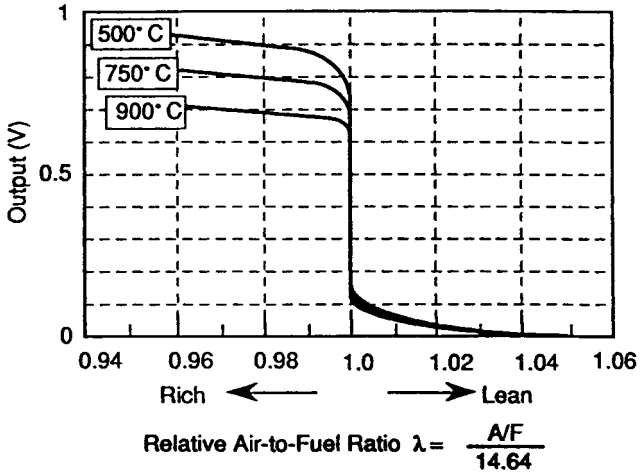

Fig. 2. A typical characteristics of a product zirconia exhaust gas oxygen sensor.

the mass air flow rate. In Section VII, the effects of transient fuel delivery dynamics are compensated. Sections VIII and IX present numerical simulation and experimental results.

II. Fuel Injection Model of Port Fuel Injection System

A schematic diagram of fuel injection control is shown in Fig. 3. The control problem is to vary the fuel-spray rate $\dot{m}_{fo}$ so that the A/F ratio remains close to stoichiometry even during a rapid throttle transient.

A simplified dynamic model [6], [8] for this problem is

$$\dot{m}_a = \dot{m}_{ai}(\alpha, m_a) - \dot{m}_{ao}(\omega_e, m_a) \tag{1}$$

$$\tau_f \ddot{m}_{fo}(t) = -\dot{m}_{fo}(t) + \dot{m}_{fc}(t - \Delta t_f). \tag{2}$$

The first equation is the air flow dynamics through the intake manifold. m_a is the mass of air in the intake manifold, α is the throttle angle, ω_e is the engine speed, $\dot{m}_{ai}$ is the air-mass-flow rate into the manifold, and $\dot{m}_{ao}$ is the air-mass-flow rate out of the manifold which is given as a function of ω_e and m_a. The mass air flow rate into the manifold $(\dot{m}_{ai})$ can be measured by a hot-wire sensor. The mass air flow rate out of the manifold $(\dot{m}_{ao})$ cannot be measured. However, during steady-state operations, $\dot{m}_{ao}$ is identical with $\dot{m}_{ai}$. Therefore, the steady-state map of $\dot{m}_{ao}$ (Fig. 4) can be obtained as a function of engine speed and manifold pressure by steady-state engine tests.

By denoting the steady-state air flow rate out of the manifold as $\dot{\hat{m}}_{ao}(m_a, \omega_e)$, the true air flow rate during transient operations can be expressed as

$$\dot{m}_{ao} = (1 + e)\dot{\hat{m}}_{ao}(m_a, \omega_e) \tag{3}$$

where e is a multiplicative error fraction. For S.I. engines, the slope of the $\dot{\hat{m}}_{ao}(m_a, \omega_e)$ map in the direction of m_a, is always positive [9]. This characteristic is exploited in the dynamic sliding mode controller design. Exhaust gas recirculation (EGR) is adopted in many of gasoline engines these days for the reduction of the NO_X pollutants. In this air flow dynamics model, exhaust gas recirculation is not included for the simplicity of the control task. However, extension of the control algorithm when EGR is in operation is not difficult.

The second equation is a first-order linear approximation of fuel delivery dynamics. The equation models pure time delay (Δt_f) in the commanded fuel injection spray rate $(\dot{m}_{fc})$. $\dot{m}_{fo}$ is the actual spray rate into the cylinder and τ_f is the fueling time constant. The pure time delay is caused by computation time delay and delays in opening the intake valves. The lag (the first-order dynamics represented by the time constant τ_f) is due to the fuel wetting/evaporation on the intake wall. In our transient fueling compensation, the fuel delivery dynamics model is not used. We simplify the dynamic equation as a simple algebraic equation, i.e.,

$$\dot{m}_{fo}(t) = \dot{m}_{fc}(t) - \dot{m}_{fot}(t) \tag{4}$$

where $\dot{m}_{fot}$ is the lost/added fueling rate due to the fuel delivery dynamics and can have either positive or negative value. A physical interpretation of $\dot{m}_{fot}$ is the lost fueling rate due to wall wetting and computational time delay, etc. The algebraic equation (4) is used in the transient fueling compensation.

III. Structure of Developed Fuel Injection Control Algorithm

The fuel injection controller consists of the dynamic sliding controller which mainly depends on the feedback sensor(oxygen sensor), and a transient fueling controller which uses mainly feedforward information (throttle angle change

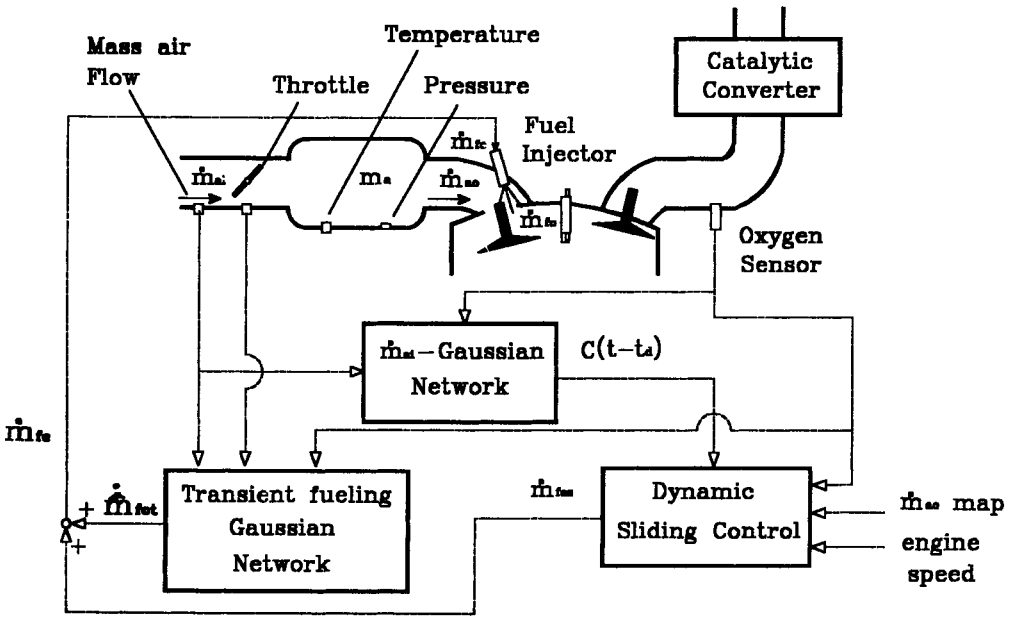

Fig. 3. Steady-state map of mass air flow rate into cylinder $(\dot{m}_{ao})$.

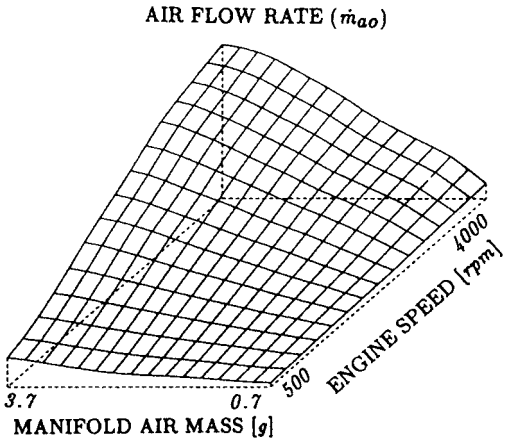

Fig. 4. Schematic diagram of developed fuel injection controller.

and mass air flow rate into the manifold) as shown in Fig. 3. The transient fueling is computed by a Gaussian network which is a function of the feedforward information. The weight in the network is corrected on-line by the oxygen sensor output. The transient fueling compensation is necessary because the dynamic sliding controller is effective only when the throttle change is not rapid. For this reason the sliding controller decides "quasisteady-state" fueling rate $(\dot{m}_{fos})$. When the throttle change is rapid, there exist undesirable peaks in the A/F ratio at both tip-in and tip-out movement of the throttle because of the fuel delivery dynamics approximated by (4) between the actual fueling command $(\dot{m}_{fc})$ and the actual fueling input rate $(\dot{m}_{fo})$. We denote the transient fueling rate to compensate the unknown lost/added fueling rate $(\dot{m}_{fot})$ as $\hat{\dot{m}}_{fot}$. The total fueling command is constructed as

$$\dot{m}_{fc} = \dot{m}_{fos} + \hat{\dot{m}}_{fot}(\dot{\alpha}, \dot{m}_{ai}). \tag{5}$$

The key idea in the control is to add or substract some amount of fueling expected to be lost or added due to the fuel delivery dynamics. The transient fueling rate is obtained from the output of the Gaussian neural network having input node variables of the throttle change rate and the mass air flow rate.

In the dynamic sliding control, the measured mass air flow rate into the manifold is utilized in calculating the control effort. A Gaussian network is used to compensate the measurement bias and the weight of the network is updated on-line by the oxygen sensor output.

IV. Dynamic Sliding Mode Control

Sliding mode control methods have been developed as a systematic way to design controllers for nonlinear plants [20], [18]. Moreover, the binary nature of the oxygen sensor output in fuel injection control is in good agreement with that of sliding mode control methods. The production oxygen sensor at the exhaust tells only the richness or leanness of the air to fuel mixture. The sensor also has a considerable time delay (t_d) because of the output measurement delay of two engine revolutions, the time delay due to the distance between exhaust ports and sensor location, and the sensor time constant. The time delay can be identified by experiments, and in our engine it is approximated by

$$t_d = 0.02 + \frac{4\pi}{\omega_e} \quad (\mathrm{s}) \tag{6}$$

where ω_e is the engine speed in rad/s. This considerable measurement time delay induces large chattering of A/F ratio in both PI control and conventional sliding control methods [6]. Dynamic sliding mode control [8] which reduces the chattering considerably is used to compute the quasisteady-state fueling rate $(\dot{m}_{fos})$. In this section, we assume the throttle change is not rapid, which means the effects of fuel delivery

dynamics are negligible. In the absence of the fuel dynamics, we can assume the fueling command ($\dot{m}_{fc}$) is the same as the actual fuel spray rate into the cylinder ($\dot{m}_{fo}$). Therefore designing $\dot{m}_{fo}$ is equivalent to designing $\dot{m}_{fos}$.

The objective of the fuel injection control is to maintain the air to fuel ratio close to 14.7 (stoichiometry ratio). Since the initial conditions are reset to near zero after the exhaust stroke, an equivalent objective is to keep

$$\frac{\dot{m}_{ao}}{\dot{m}_{fo}} = 14.7 = \beta. \tag{7}$$

Computing the rate of fuel to be injected is not trivial because the mass air flow rate into the cylinder, $\dot{m}_{ao}$, can not be measured. A sliding surface is defined as

$$s = \dot{m}_{ao} - \beta \dot{m}_{fo}. \tag{8}$$

Then the control objective is to maintain s close to zero. The binary output from the oxygen sensor y is expressed as $y(t) = \operatorname{sgn}(s(t - t_d))$.

The sliding surface is rewritten as

$$s = (1 + e)\dot{\hat{m}}_{ao} - \beta \dot{m}_{fo}. \tag{9}$$

Differentiation of the sliding surface yields

$$\dot{s} = \frac{\partial \dot{\hat{m}}_{ao}}{\partial m_a}\dot{m}_a + \frac{\partial \dot{\hat{m}}_{ao}}{\partial \omega_e}\dot{\omega}_e \ddot{\hat{m}}_{ao} + \dot{e}\dot{\hat{m}}_{ao} - \beta \ddot{m}_{fo}.$$

If $\dot{m}_{fo}$ is chosen to satisfy the following equation:

$$\beta \ddot{m}_{fo} = -\beta \frac{\partial \dot{\hat{m}}_{ao}}{\partial m_a}\dot{m}_{fo} + \left(\frac{\partial \dot{\hat{m}}_{ao}}{\partial m_a}\dot{m}_{ai} + \frac{\partial \hat{m}_{ao}}{\partial \omega_e}\right) + ly \tag{10}$$

the following closed-loop dynamics of the sliding surface results:

$$\dot{s} = -\frac{\partial \dot{\hat{m}}_{ao}}{\partial m_a}s + e\ddot{\hat{m}}_{ao} + \dot{e}\dot{\hat{m}}_{ao} - ly \tag{11}$$

where l is a positive feedback gain. In the above derivation, (1) has been used. Since the slope $\partial \dot{\hat{m}}_{ao}/\partial m_a$ is always positive [9], the resulting closed-loop system is much faster than that of sliding mode control, which is given as (12)

$$\dot{s} = e\ddot{\hat{m}}_{ao} + \dot{e}\dot{\hat{m}}_{ao} - ly. \tag{12}$$

It can be shown that the chattering magnitude of A/F ratio in dynamic sliding mode control is only 20% of that of sliding mode control [8].

In a quasisteady state, the control input $\dot{m}_{fos}$ is the same as $\dot{m}_{fo}$, which is given by integrating (10), thus the term "dynamic" controller

$$\dot{m}_{fo}(t) = \dot{m}_{fo}(0) + \frac{1}{\beta}\int_0^t \left[\frac{\partial \dot{\hat{m}}_{ao}}{\partial m_a}(\dot{m}_{ai} - \beta \dot{m}_{fo}(\tau)) + \frac{\partial \dot{\hat{m}}_{ao}}{\partial \omega_e}\dot{\omega}_e\right] d\tau + \frac{1}{\beta}\int_0^t ly(\tau)\, d\tau.$$

This control law represents a good way to combine the speed-density method and the mass-air-flow-meter (MAFM) method.

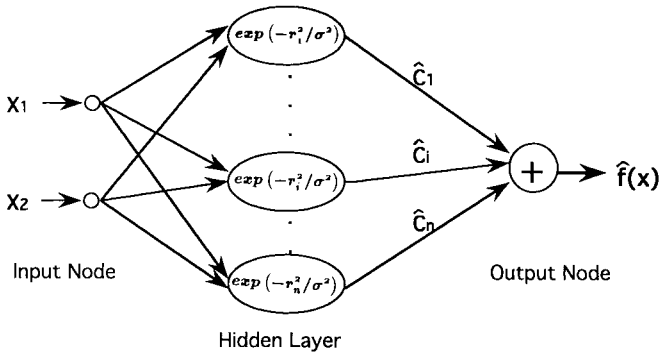

Fig. 5. Neural-network construction of $\hat{f}(x)$.

This control law utilizes the measured value of the mass air flow rate into the manifold like the MAFM method, and the information derived from the steady-state $\dot{\hat{m}}_{ao}$ map similar to the one used in the speed density method.

V. Direct Adaptive Control Using Gaussian Neural Network

In this section, a direct adaptive control method using Gaussian network [16] is introduced which is similar to adaptive sliding mode control. This method is used in the compensation of fuel delivery dynamics and the measurement bias of the mass air flow rate into the manifold.

Consider a nonlinear dynamic system in the canonical form

$$x^{(n)}(t) = f(x(t), \dot{x}(t), \cdots, x^{(n-1)}(t)) + bu(t) \tag{13}$$

where f is an unknown function, $u(t)$ the input, and b a nonzero known constant. The unknown function f can be approximated by $f_A(x)$ which is expanded by the Gaussian functions [16]

$$f_A(x) = \sum_{i=1}^{m} c_i \cdot \exp\left(-\frac{r_i(x)^2}{\sigma^2}\right) \tag{14}$$

where m is the number of the sampling points in the state space, σ is a positive constant [16], c_i are constant coefficients, and $r_i(x)$ are the distances from the current state x to the fixed sampling points (nodes) in the state space. The construction of $f_A(x)$ can be viewed as a neural network with one hidden layer (Fig. 5). For a sufficiently smooth function $f(x)$, it is shown that $f_A(x)$ can uniformly approximate $f(x)$ to a chosen degree of accuracy using finite numbers of the Gaussian functions, i.e.,

$$f(x) = f_A(x) + e_1(x) \tag{15}$$

where the approximation error $e_1(x)$ satisfying $|e_1(x)| < \epsilon$ for a given constant ϵ [16]. We define $\hat{f}_A(x)$ as an estimate of $f_A(x)$

$$\hat{f}_A(x) = \sum_{i=1}^{m} \hat{c}_i \cdot \exp\left(-\frac{r_i(x)^2}{\sigma^2}\right) \tag{16}$$

where $\hat{c}_i$ are the estimates of the true coefficients c_i.

A sliding surface s and a Lyapunov function V are chosen as

$$s = x^{(n-1)}(t) + \lambda_{n-2}x^{(n-2)}(t) + \cdots + \lambda_1\dot{x}(t) + \lambda_0 x(t) \tag{17}$$

$$V = \frac{1}{2}\left(s^2 + \frac{1}{g}\sum_{i=1}^{m}\tilde{c}_i^2\right) \tag{18}$$

where λ_i are positive constants that makes $s = 0$ stable, $\tilde{c}_i = c_i - \hat{c}_i$, and g is a positive constant. Differentiation of V yields

$$\dot{V} = s(f + bu + \lambda_{n-2}x^{(n-1)}(t) + \cdots + \lambda_0\dot{x}(t)) - \frac{1}{g}\sum_{i=1}^{m}\tilde{c}_i\dot{\hat{c}}_i$$

where $\dot{\tilde{c}}_i = -\dot{\hat{c}}_i$ is used. Choosing the control input u satisfying

$$bu = -\hat{f} - \lambda_{n-2}x^{(n-1)}(t) - \cdots - \lambda_0\dot{x}(t) - Ks \tag{19}$$

yields

$$\dot{V} = -Ks^2 + e_1(x)s + \sum_{i=1}^{m}\left(s\cdot\exp\left(-\frac{r_i(x)^2}{\sigma^2}\right) - \frac{1}{g}\dot{\hat{c}}_i\right)\tilde{c}_i \tag{20}$$

where K is a feedback gain. Choosing an adaptation law for the coefficients c_i as

$$\dot{\hat{c}}_i = g\cdot s\cdot\exp\left(-\frac{r_i(x)^2}{\sigma^2}\right) \tag{21}$$

gives

$$\dot{V} = -Ks^2 + e_1(x)s. \tag{22}$$

Therefore $|s| > \frac{\epsilon}{K}$ guarantees $\dot{V} < 0$ since $|e_1(x)| < \epsilon$, which means the Lyapunov function is bounded and the absolute value of the sliding surface is bounded by ϵ/K.

VI. Measurement Bias Compensation in Mass Air Flow Rate into Manifold

Dynamic sliding mode control is very sensitive to the measurement bias in the mass air flow rate into the manifold $(\dot{m}_{ai})$ since the closed-loop dynamics are very fast, and the term containing $\dot{m}_{ai}$ acts as an exciting term in the closed-loop dynamics. $\dot{m}_{ai}$ is measured by a hot wire sensor, and an one-dimensional nonlinear table is used to relate the sensor output voltage to the actual mass air flow rate since the hot wire sensor characteristic is not quite linear. Also, the characteristics of the hot wire sensor change with the ambient temperature and time. Therefore the conversion table needs to be changed on line to give better correlation between the sensor output and the mass air flow rate. In this section, the measured mass air flow rate $\dot{m}_{aim}$ is corrected by a one-dimensional function. This function is adapted on-line using a Gaussian neural network.

The corrected or estimated value of the mass air flow rate $(\dot{\hat{m}}_{ai})$ is constructed as

$$\dot{\hat{m}}_{ai}(t) = \dot{m}_{aim}(t)(1 + \hat{C}(t - t_d)) \tag{23}$$

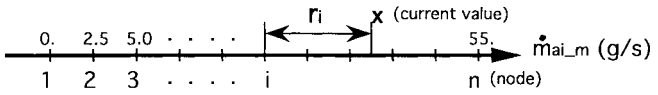

Fig. 6. Neural-network mesh of mass air flow rate into cylinder.

where $\hat{C}(t) = \Sigma_{i=1}^{m}\hat{d}_i(t)\exp(-(r_i(t)^2/\sigma^2))$. Here $r_i(t)$ are the distance from the current measurement $\dot{m}_{aim}(t)$ to i_{th} node on a $\dot{m}_{aim}$ axis (see Fig. 6), σ is a constant, and $\hat{d}_i$ are the estimates of true parameters d_i. The reason for $\hat{C}(t - t_d)$ being used rather than $\hat{C}(t)$ is that the oxygen sensor output is available up to $t - t_d$ at time t. $\hat{C}(t - t_d)$ is a value which is calculated based on the oxygen sensor measurement up to time $t - t_d$. The true mass air flow rate $\dot{m}_{ai}$ can be expressed as

$$\dot{m}_{ai}(t) = \dot{m}_{aim}(t)[1 + C(t - t_d) + e_m] \tag{24}$$

where e_m is the approximation error of the neural network.

We choose the sliding surface (s) and a Lyapunov function (V) as

$$s = \dot{m}_{ao} - \beta\dot{m}_{fo} \tag{25}$$

$$V = |s| + \frac{1}{2\rho}\sum_{i=1}^{m}\tilde{d}_i(t)^2 \tag{26}$$

where ρ is a positive constant and $\tilde{d}_i = d_i - \hat{d}_i$. When s is not zero, differentiation of V becomes

$$\dot{V} = \dot{s}\,\mathrm{sgn}(s) + \frac{1}{\rho}\sum_{i=1}^{m}\dot{\tilde{d}}_i(t)\tilde{d}_i(t). \tag{27}$$

Under the control given as

$$\beta\ddot{m}_{fo} = -\beta\frac{\partial\dot{\hat{m}}_{ao}}{\partial m_a}\dot{m}_{fo} + \left(\frac{\partial\dot{\hat{m}}_{ao}}{\partial m_a}\dot{\hat{m}}_{ai}(t) + \frac{\partial\dot{\hat{m}}_{ao}}{\partial\omega_e}\right) + ly \tag{28}$$

(which is the same as the dynamic sliding control (10), except for the $(\partial\dot{\hat{m}}_{ao}/\partial m_a)\dot{\hat{m}})_{a_i}$ term), $\dot{s}$ becomes

$$\dot{s} = -\frac{\partial\dot{\hat{m}}_{ao}}{\partial m_a}s + e\ddot{m}_{ao} + \dot{e}\dot{\hat{m}}_{ao} + \frac{\partial\dot{\hat{m}}_{ao}}{\partial m_a}\dot{\hat{m}}_{a_i}(t) - ly. \tag{29}$$

The estimation error in $\dot{m}_{a_i}$ is expressed as

$$\begin{aligned}\dot{\tilde{m}}_{ai}(t) &= \dot{m}_{ai}(t) - \dot{\hat{m}}_{ai}(t)\\ &= \dot{m}_{aim}(t)\tilde{C}(t - t_d) + \dot{m}_{aim}(t)e_m\end{aligned} \tag{30}$$

where $\tilde{C}(t - t_d) = C(t - t_d) - \hat{C}(t - t_d)$. This estimation error can also be represented by

$$\dot{\tilde{m}}_{ai}(t) = \dot{m}_{aim}(t)\tilde{C}(t) + \dot{m}_{aim}(t)(\tilde{C}(t - t_d) - \tilde{C}(t) + e_m). \tag{31}$$

Putting (29) into (27) yields

$$\begin{aligned}\dot{V} = &-\frac{\partial\dot{\hat{m}}_{ao}}{\partial m_a}|s| + \mathrm{sgn}(s)(e_2 - ly) + \sum_{i=1}^{m}\tilde{d}_i\\ &\cdot\left[\mathrm{sgn}(s(t))\frac{\partial\dot{\hat{m}}_{ao}}{\partial m_a}\dot{m}_{aim}(t)\exp\left(-\frac{r_i(t)^2}{\sigma^2}\right) - \frac{1}{\rho}\dot{\hat{d}}_i(t)\right]\end{aligned}$$

where $e_2 = e\ddot{\hat{m}}_{ao} + \dot{e}\dot{\hat{m}}_{ao} + (\partial\dot{\hat{m}})_{ao}/\partial m_a)\dot{m}_{aim}(\tilde{C}(t-t_d) - \tilde{C}(t) + e_m)$.

Choosing the adaptation law as

$$\dot{\hat{d}}_i = \rho \operatorname{sgn}(s(t)) \frac{\partial \dot{\hat{m}}_{ao}}{\partial m_a} \dot{m}_{aim}(t) \exp\left(-\frac{r_i(t)^2}{\sigma^2}\right) \tag{32}$$

yields

$$\dot{V} = -\frac{\partial \dot{\hat{m}}_{ao}}{\partial m_a}|s| + \operatorname{sgn}(s)(e_2 - ly). \tag{33}$$

After time shifting by t_d, we can express the adaptation law as

$$\dot{\hat{d}}_i(t-t_d) = \rho \operatorname{sgn}(s(t-t_d)) \frac{\partial \dot{\hat{m}}_{ao}}{\partial m_a}(t-t_d)\dot{m}_{aim}(t-t_d) \cdot \exp\left(-\frac{r_i(t-t_d)^2}{\sigma^2}\right). \tag{34}$$

Now the adaptation law is implementable at time t, and the innovated $\hat{d}_i(t-t_d)$ is used to calculate $\hat{C}(t-t_d)$ in (23). The terms $e\ddot{\hat{m}}_{ao} + \dot{e}\dot{\hat{m}}_{ao}$ in e_2 represents the estimation error of the change of the mass flow rate into the cylinders $(\ddot{m}_{ao})$. Since the change is bounded and so is our estimate, we can conclude the estimation error is bounded. The approximation error e_m and $(\tilde{C}(t-t_d) - \tilde{C}(t))$ are also bounded quantities. Therefore $\operatorname{sgn}(s)(e_2 - ly)$ in (33) is bounded, and $\dot{V} < 0$ when $|s| > (|e_2| + l)/(\partial\dot{\hat{m}}_{ao}/\partial m_a)$. We finally conclude the absolute value of the sliding surface s is bounded under the control. The quasisteady-state fueling command is obtained from integrating (28).

The adaptation algorithm is considered to be effective not only for the variation of the air flow rate sensor characteristic, but also to slowly varying A/F ratio disturbances such as one resulting from injector aging.

VII. Transient Fuel Compensation

As will be seen in the experimental section, the dynamic sliding controller shows good performance when the throttle angle change is not rapid. However, rapid change of the throttle angle cause sharp peaks in the A/F ratio as a result of the fuel delivery dynamics (Fig. 15). In this section, the fuel flow rate command is corrected to compensate for the unknown fuel delivery dynamics. Since the transient fuel delivery dynamics include pure time delay in the input, it is necessary to employ a feedforward control input using variables that are faster than the mass air flow rate into the cylinder $(\dot{m}_{ao})$. The positive or negative amount of the transient fueling rate $(\dot{m}_{fot})$ is approximated as a function of the rate of throttle change $(\dot{\alpha})$ and the mass air flow rate into the manifold $(\dot{m}_{ai})$. The reason for choosing $\dot{\alpha}$ as an independent variable is that the rate of throttle change is faster than the mass air flow rate out of the manifold $(\dot{m}_{ao})$, and it roughly decides the sign of the transient fueling rate $(\dot{m}_{fot})$. The mass air flow rate into the manifold $(\dot{m}_{ai})$ is selected because $\dot{m}_{ai}$ is faster than $\dot{m}_{ao}$, and is similar to $\dot{m}_{ao}$. The rate of the throttle change $\dot{\alpha}$ was obtained by low pass filtering the numerical approximation, $(\alpha(t) - \alpha(t-t_s))/t_s$ where t_s is the sampling time.

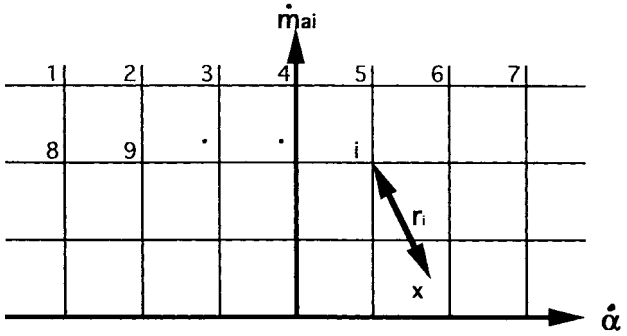

Fig. 7. Neural-network mesh for transient fueling.

In this section, the quasisteady-state control input $(\dot{m}_{fos})$ is combined with the transient fueling input $(\dot{\hat{m}}_{fot})$. The total fuel command to the injector $(\dot{m}_{fc})$ is

$$\dot{m}_{fc} = \dot{m}_{fos} + \dot{\hat{m}}_{fot}(\dot{\alpha}, \dot{m}_{ai}) \tag{35}$$

where $\dot{m}_{fos}$ is the steady-state fueling rate of the previous section, which is obtained by integrating (28) and $\dot{\hat{m}}_{fot}$ is our estimate of the additional fuel rate required to compensate for the lost/added fueling rate. Putting (35) into (4) yields

$$\dot{m}_{fo} = \dot{m}_{fos} + \dot{\tilde{m}}_{fot} \tag{36}$$

where $\dot{\tilde{m}}_{fot} = \dot{\hat{m}}_{fot} - \dot{m}_{fot}$. The sliding surface s is defined as

$$s = \dot{m}_{ao} - \beta\dot{m}_{fo} \tag{37}$$

or equivalently

$$s = \dot{m}_a o - \beta(\dot{m}_{fos} + (\dot{\hat{m}}_{fot} - \dot{m}_{fot})). \tag{38}$$

Here we construct the time derivative of $\dot{\hat{m}}_{fot}$ as

$$\ddot{\hat{m}}_{fot}(t) = \sum_{i=1}^{m} \hat{c}_i(t-t_d) \exp\left(-\frac{r_i(t-t_d)^2}{\sigma^2}\right) \tag{39}$$

where r_i is the Euclidian distance from the current state to i_{th} node on a $(\dot{\alpha}, \dot{m}_{ai})$ grid (see Fig. 7), and σ is a constant. $\hat{c}_i$ are our estimates of the "true" constant values c_i. We define $F_t(t) = \Sigma_{i=1}^{m}\ c_i(t)\exp(-(r_i(t)^2/\sigma^2))$ and $\hat{F}_t(t) = \Sigma_{i=1}^{m} \hat{c}_i(t)\exp(-(r_i(t)^2/\sigma^2))$. Then $\ddot{m}_{fot}$ can be expressed as

$$\ddot{m}_{fot} = F_t(t-t_d) + e_t \tag{40}$$

where e_t is the approximation error. A Lyapunov function is chosen as

$$V = |s| + \frac{1}{2g}\sum_{i=1}^{m} \tilde{c}_i^2(t) \tag{41}$$

where g is a positive constant. The absolute function is used because only the sign of s is available. When s is not zero, differentiation of V becomes

$$\dot{V} = \dot{s}\operatorname{sgn}(s) + \frac{1}{g}\sum_{i=1}^{m} \tilde{c}_i\dot{\tilde{c}}_i \tag{42}$$

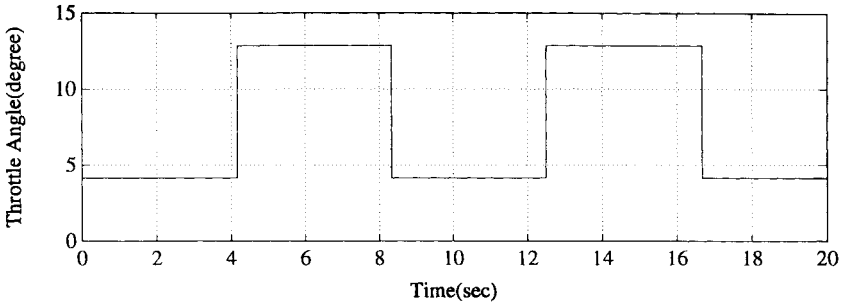

Fig. 8. Throttle angle pattern in A/F ratio control simulation.

where $\tilde{c}_i = \hat{c}_i - c_i$. Combining the quasisteady-state control (28) and the adaptation law (34) with (39) and (40) yields the expression for $\dot{s}$

$$\dot{s} = -\frac{\partial \dot{\hat{m}}_{ao}}{\partial m_a} s - \beta \frac{\partial \dot{\hat{m}}_{ao}}{\partial m_a} \dot{\hat{m}}_{fot} + e_3 - ly - \beta \tilde{F}_t(t - t_d) \tag{43}$$

where $e_3 = e_2 + \beta e_t$ and $\tilde{F}_t(t-t_d) = \hat{F}_t(t-t_d) - F_t(t-t_d)$. Since the error in the transient fueling rate e_t is absolutely bounded, so is e_3. Using (43) and $\dot{\tilde{c}}_i = \dot{\hat{c}}_i, \dot{V}$ becomes

$$\dot{V} = -\frac{\partial \dot{\hat{m}}_{ao}}{\partial m_a}|s| + \operatorname{sgn}(s)(e_3 + \beta(\tilde{F}(t) - \tilde{F}(t-t_d)) - ly) - \sum_{i=1}^{m} \tilde{c}_i \left[\beta \exp\left(-\frac{r_i(x)^2}{\sigma^2} \right) \operatorname{sgn}(s) - \frac{1}{g} \dot{\hat{c}}_i \right]. \tag{44}$$

Choosing the adaptation laws for the coefficients $c_i(t-t_d)$ as

$$\dot{\hat{c}}_i(t - t_d) = \operatorname{sgn}(s(t-t_d)) \cdot g \cdot \beta \cdot \exp\left(-\frac{r_i(t-t_d)^2}{\sigma^2} \right) \tag{45}$$

yields

$$\dot{V} = -\frac{\partial \dot{\hat{m}}_{ao}}{\partial m_a}|s| + \operatorname{sgn}(s)(e_3 + \beta(\tilde{F}(t) - \tilde{F}(t-t_d)) - ly) \tag{46}$$

where $(\partial \dot{\hat{m}}_{ao}/\partial m_a) > 0$. Thus, $\dot{V} < 0$ is achieved for

$$|s| > \frac{|e_3 + \beta(\tilde{F}(t) - \tilde{F}(t-t_d))| + l}{\dfrac{\partial \dot{\hat{m}}_{ao}}{\partial m_a}} \tag{47}$$

and the absolute value of the sliding surface is bounded. Our transient control $\dot{\hat{m}}_{fot}$ is given by integrating (39).

The total control input is expressed as

$$\dot{m}_{fc}(t) = \dot{m}_{fos}(t) + \int_0^t \hat{F}_t(\tau - t_d)\, d\tau. \tag{48}$$

VIII. Simulation of Dynamic Sliding Control

In this section, numerical simulation of dynamic sliding control is executed to verify its fast closed-loop dynamics and small chattering magnitudes. The compensation technique of fuel delivery dynamics and measurement bias of $\dot{m}_{a_i}$ was implemented in experiments with dynamic sliding mode control.

The model error in the mass air flow rate into the cylinder $(\dot{m}_{ao})$ is taken to be

$$e(t) = 0.1 \sin(\pi t) \tag{49}$$

which represents $\pm 10\%$ error with 0.5-Hz frequency.

The measurement time delay of the oxygen sensor is the transportation time for an amount of air to enter the cylinders, go through combustion, and travel down to the sensor plus sensor response time. The sensor time delay $t_d = 0.02 + 4\pi/\omega_e(t)$ was used in simulations. The throttle was varied as shown in Fig. 8 to simulate fast acceleration and deceleration which allows the engine to be operated between 1000 and 4000 r/min.

First the performance of dynamic sliding mode control was demonstrated for the case with modeling error but without measurement time delay. The simulation result shown in Fig. 9 shows almost exact regulation of the A/F ratio around 14.7 except when the throttle angle changes abruptly. The sharp peaks are due to the computational time delay in control.

Next, dynamic sliding mode control was applied to the plant with the time delay. Fig. 10 shows that this controller is robust to the time delay and that most of the time the A/F ratio is within the $\pm 1.4\%$ error boundary from stoichiometry.

IX. Experimental Results

Some experimental results reported in the literature are obtained for tip-in/tip-out throttle modes with the engine speed fixed by a dynamometer. However, in many cases, the engine speed changes dramatically during the transient throttle modes, since such throttle modes generally accompany gear shifting. Other results are obtained when the tip-in/tip-out modes are in the large throttle opening zone. Since the intake manifold air pressure (or air mass) reaches more than 80% of the atmospheric (or full-open throttle) pressure before the throttle is half-opened, the large change of the throttle angle in the large throttle opening zone gives only mild variations of the manifold pressure. In this study, all the experimental results are obtained under more severe and more realistic conditions: the dynamometer load is fixed where dynamometer inertia is the only external inertia; and the throttle varies from a small throttle angle.

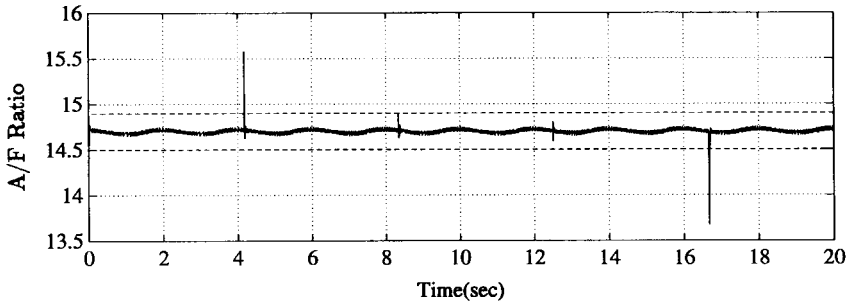

Fig. 9. A/F ratio by dynamic sliding mode control without measurement time delay (simulation).

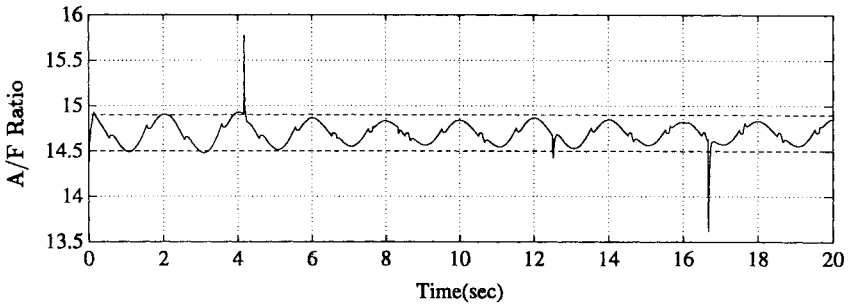

Fig. 10. A/F ratio by dynamic sliding mode control with measurement time delay (simulation).

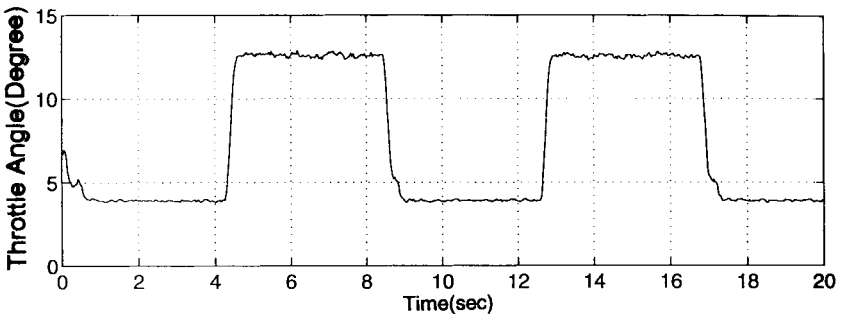

Fig. 11. Throttle angle pattern in A/F ratio control experiments.

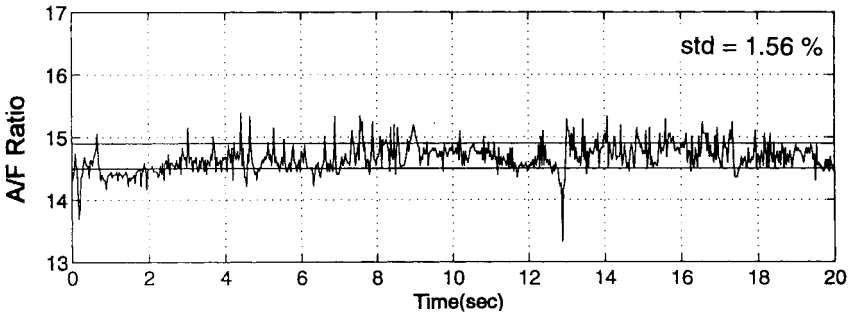

Fig. 12. A/F ratio controlled by Gaussian network sliding control.

The suggested controller was evaluated at the University of California, Berkeley engine dynamometer test rig, and compared with a production ECM controller. The engine used for the test is a 3.8-l V-6 sequential port-injection S.I. engine. The controllers were implemented using a 33-MHz-CPU PC-386 and a MicroSoft Quick-C compiler at 10-ms loop-time, and premium gasoline was used. The throttle was controlled by a stepper motor which has a maximum speed of 900 steps/s and a motor controller which allows the throttle to be changed abruptly in less than 0.1 s. The fuel injector driver was built using six LM322N timer chips which modulate the injection pulse width from the production ECM when it is needed to run

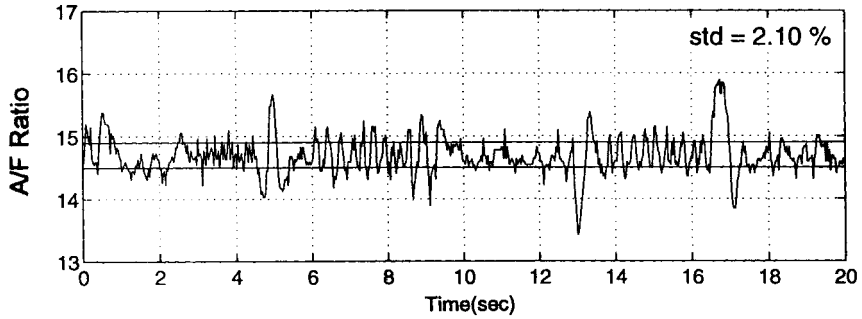

Fig. 13. A/F ratio controlled by production ECM.

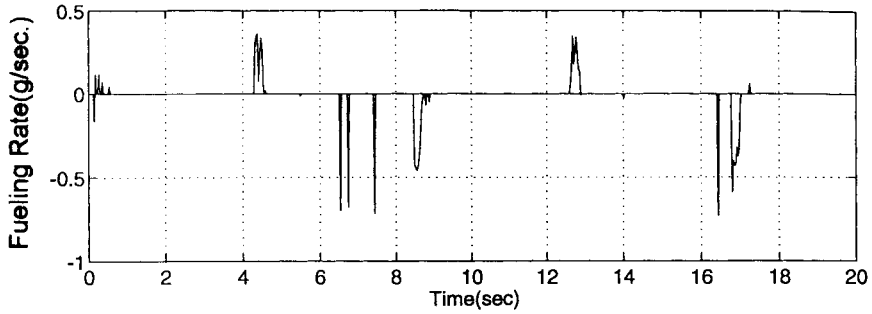

Fig. 14. Compensated transient fueling rate in Gaussian network sliding control.

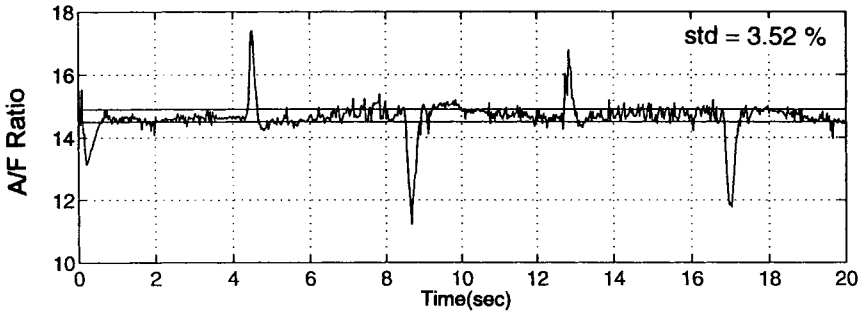

Fig. 15. A/F ratio by Gaussian network sliding control without transient fuel compensation.

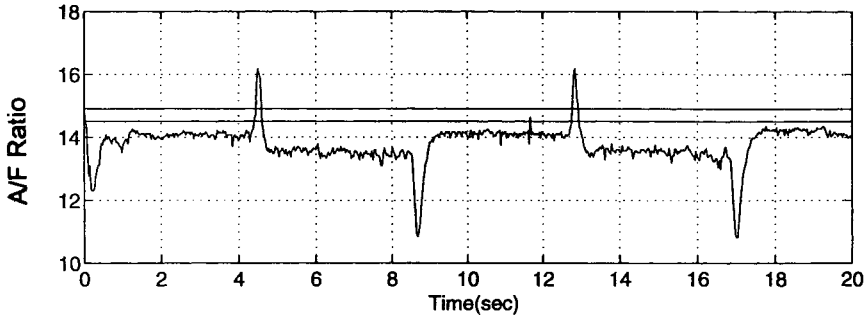

Fig. 16. A/F ratio by dynamic sliding control (no compensation of measurement error of $\dot{m}_{ai}$ and transient fuel).

the developed controller. Mass air flow rate through the throttle body, manifold pressure, and temperature, and the oxygen in the exhaust gas were measured using typical production engine sensors. The engine speed was measured by using a magnetic pick-up installed on the engine flywheel. A linear oxygen sensor (NISSAN model PLR-1) installed in the exhaust pipe was used only to monitor control performance.

The initial weights of the mass air flow rate Gaussian network were chosen to have the correction factor $\hat{C}(t-t_d)$ equal to zero. The initial weights of the transient fueling Gaussian network were all zero, which means the transient fueling compensation is zero at the initial time. In other words, no prior knowledge of the weights are given and the weights of the two networks have meaningful values as the on-line learning process continues. The nodes of the mass air flow rate network are evenly spaced from 0 to 55 g/s. with 2.5 g/s. spacing. The nodes of the transient fueling network are spaced from 0 to 60 g/s. in the $\dot{m}_{ai}$ axis with spacing of 10 g/s. and from -60 to $+60$ deg/s in the $\dot{\alpha}$ axis with spacing of 10 deg/s.

The throttle variation in the experiment is shown in Fig. 11. With the external load from a dynamometer fixed to 67.7 N-m, the throttle variation induces large variations of the manifold pressure. During the throttle variation, the A/F ratio (Fig. 12) controlled by the developed controller gives about 30% smaller standard deviation than the result of the production ECM (Fig. 13). The result (Fig. 12) of the proposed controller is obtained after several 20 s. learning trials in both the mass air flow rate and the transient Gaussian networks with similar throttle variations as the throttle variation in Fig. 11. The learning process is the on-line adaptation of the constants $\hat{c}_i$ of the transient fueling rate map, $\dot{m}_{fot}(\dot{\alpha}, \dot{m}_{ai})$ and the constants $\hat{d}_i$ of the mass air flow rate map. Comparing Figs. 12 and 13, we can see the A/F ratio variation of the proposed control has higher frequency contents than that of the ECM result, which means that the closed-loop dynamics of the proposed control is faster than that of the ECM controller. This is one of the reasons that the proposed controller results a smaller standard deviation than that of the ECM.

Fig. 14 shows the transient fueling rate command $(\dot{\hat{m}}_{fot})$ of the proposed controller, which gives the A/F ratio of Fig. 12. Fig. 15 shows the A/F ratio when the transient fuel compensation is not accompanied by the dynamic sliding control. The sharp peaks of the A/F ratio demonstrates the necessity of the transient fueling compensation. Fig. 16 shows the results of the A/F ratio of the proposed controller when both the transient fueling compensation and the mass air flow rate bias adaptation are not accompanied. It is also seen that A/F ratio has significant drift from stoichiometry with large transient peaks.

Experimental results during engine warming up confirm that the mass air flow meter characteristics changes with the manifold temperature. In future work, the manifold temperature will be included as an independent variable of the mass air flow rate network.

X. Conclusion

The A/F ratio control of S.I. engines have been conducted using a dynamic sliding control method and Gaussian neural networks. The simulation and experimental results show that the closed-loop system is much faster than those of the conventional sliding mode control and the production ECM controller. It is verified that the developed controller gives about 30% smaller standard deviation than that of the production ECM. The new control method suggests a way to avoid the time consuming gain tuning process by using an on-line learning algorithm. The transient fueling compensation and the mass air flow rate correction algorithm can be used with other types of engines and is insensitive to aging since the technique identifies the engine characteristics on-line.

References

[1] C. F. Aquino, "Transient A/F control characteristics of the five-liter central fuel injection engine," SAE Paper 810494, 1981.

[2] P. C. Baruah, "A simulation model for transient operation of spark-ignition engines," SAE Paper 900682, 1990.

[3] R. P. Canale, C. R. Carlson, S. R. Winegarden, and D. L. Miles, "General motors phase II catalyst system," SAE Paper 780205, 1978.

[4] J. F. Cassidy, M. Athans, and W.-H. Lee, "On the design of electronic automotive engine controls using linear quadratic control theory," *IEEE Trans. Automat. Contr.*, vol. AC-25, pp. 901–910, Oct. 1981.

[5] C.-F. Chang, N. P. Fekete, and J. D. Powell, "Engine air-fuel ratio using an event-based observer," SAE Paper 930766, 1993.

[6] D. Cho and J. K. Hedrick, "A nonlinear controller design method for fuel-injected automotive engines," *ASME Trans. J. Engine, Gas Turbines, and Power*, July 1988.

[7] ——, "Sliding mode fuel-injection controller: Its advantages," *ASME J. Dynamic Syst., Measurement, Contr.*, vol. 113, no. 3, pp. 537–541, Sept. 1991.

[8] S. B. Choi and J. K. Hedrick, "An observer-based controller design method for automotive fuel-injection systems," in *Proc. ACC*, 1993, pp. 2567–2571.

[9] ——, "An observer-based controller design method for improving air/fuel characteristics of S.I. engines: Theory and experiment," in *ASME WAM, Symp. Transportation Syst.*, 1993.

[10] D. J. Dobner, "A mathematical engine model for development of dynamic engine control," SAE Paper 800054, 1980.

[11] J. C. Doyle and G. Stein, "Multivariable feedback design: Concepts for a classical/modern synthesis," *IEEE Trans. Automat. Contr.*, vol. AC-26, Feb. 1981.

[12] C. D. Falk and J. J. Mooney, "Three-way conversion catalysts: Effect of closed-loop feedback control and other parameters on catalyst efficiency," SAE Paper 800462, 1980.

[13] E. Hendricks and S. C. Sorenson, "SI engine controls and mean value engine modeling," SAE Paper 910258, 1991.

[14] S. D. Hires and M. T. Overington, "Transient mixture strength excursions—An investigation of their causes and the development of a constant mixture strength fueling strategy," SAE Paper 810495, 1981.

[15] R. D. Matthews *et al.*, "Intake and ECM submodel improvements for dynamic SI engine models: Examination of tip-in/tip-out," SAE Paper 910074, 1991.

[16] R. M. Sanner and J. J. E. Slotine, "Gaussian networks for direct adaptive control," *IEEE Trans. Neural Networks*, vol. 3, 1992.

[17] H. Shiraishi *et al.*, "CMAC neural-network controller for fuel-injection systems," *IEEE Trans. Contr. Syst. Technol.*, vol. 3, 1995.

[18] J. J. E. Slotine and W. Li, *Applied Nonlinear Control.* Englewood Cliffs, NJ: Prentice-Hall, 1991.

[19] Y. Sogawa *et al.*, "Improvement of engine transient characteristics using an induction chamber model," *Int. J. Vehicle Design*, vol. 10, no. 5, 1989.

[20] V. I. Utkin (trans. by A. Parnakh), *Sliding Modes and Their Application in Variable Structure System.* Moscow, Russia: MIR, 1978.

[21] M. Won, "Multiple surface sliding control with application to engine control," Ph.D dissertation, Univ. California at Berkeley, 1995.